Mineralogical Magazine (2023), **87**, 582–590
doi:10.1180/mgm.2023.34

CAMBRIDGE UNIVERSITY PRESS

Article

Holubite, $Ag_3Pb_6(Sb_8Bi_3)_{\Sigma 11}S_{24}$, from Kutná Hora, Czech Republic, a new member of the andorite branch of the lillianite homologous series

Richard Pažout[1], Jakub Plášil[2], Michal Dušek[2], Jiří Sejkora[3] and Zdeněk Dolníček[3]

[1]University of Chemistry and Technology Prague, Technická 5, Praha 6, 166 28, Czech Republic; [2]Institute of Physics of the Czech Academy of Sciences, Cukrovarnická 10/112, 182 21, Praha 8, Czech Republic and [3]Department of Mineralogy and Petrology, National Museum, Cirkusová 1740, 193 00, Praha 9, Czech Republic

Abstract

A new mineral species, holubite, ideally $Ag_3Pb_6(Sb_8Bi_3)_{\Sigma 11}S_{24}$, has been found at Kutná Hora ore district, Czech Republic. The mineral is associated with other lillianite homologues (gustavite, terrywallaceite, vikingite and treasurite) most frequently as grain aggregates and replacement rims of earlier Ag–Pb–Bi minerals, growing together in aggregates up to 200 × 50 μm. It typically occurs in a close association with Ag,Bi-bearing galena and terrywallaceite. Holubite is opaque, steel-grey in colour and has a metallic lustre, the calculated density is 5.899 g/cm^3. In reflected light holubite is greyish white and bireflectance and pleochroism are weak with grey tints. Anisotropy is weak to medium with grey to bluish-grey rotation tints. Internal reflections were not observed. Electron microprobe analyses yielded an empirical formula, based on 44 atoms per formula unit (apfu) of $(Ag_{3.03}Cu_{0.03})_{\Sigma 3.06}(Pb_{6.19}Fe_{0.02}Cd_{0.01})_{\Sigma 6.22}(Sb_{7.71}Bi_{2.90})_{\Sigma 10.61}S_{24.12}$. Its unit-cell parameters are: $a = 19.374(4)$, $b = 13.201(3)$, $c = 8.651(2)$ Å, $\beta = 90.112(18)°$, $V = 2212.5(9)$ Å^3, space group $P2_1/n$ and $Z = 2$. Holubite is a new member of the andorite branch of the lillianite homologous series with $N = 4$. The structure of holubite contains two Pb sites with a trigonal prismatic coordination, eight distinct octahedral sites, of which one is a mixed (Bi,Ag) site and one is a mixed (Sb,Pb) site, and twelve anion sites. Holubite is defined as a lillianite homologue with the three following requirements: $N = 4$, L% [$Ag^+ + (Bi^{3+},Sb^{3+}) \leftrightarrow 2\ Pb^{2+}$ substitution] ≈ 70% and approximately one quarter to one third at.% of antimony is replaced by bismuth [Bi/(Bi+Sb) ≈ 0.26–34]. The new mineral has been approved by the Commission on New Minerals, Nomenclature and Classification of the International Mineralogical Association (IMA2022-112) and named after Milan Holub, a key Czech geologist and specialist in the Kutná Hora ore district.

Keywords: holubite; new mineral; lillianite homologue; mixed Sb–Bi member; Kutná Hora; Czech Republic

(Received 14 March 2023; accepted 28 April 2023; Accepted Manuscript published online: 11 May 2023; Associate Editor: Oleg I Siidra)

Introduction

A new sulfosalt mineral species, holubite, ideally $Ag_3Pb_6(Sb_8Bi_3)_{\Sigma 11}S_{24}$, has been found on medieval mine dumps of the Staročeské pásmo Lode of the historic Kutná Hora Ag–Pb–Zn ore district, Central Bohemia, Czech Republic. The mineral is named after Milan Holub (born 1938), a Czech geologist and the author of the crucial modern geological work on geology of the Kutná Hora deposit "The Polymetallic Mineralization of Kutná Hora Ore District" (Holub *et al.*, 1982). Milan Holub is the author of over 30 publications in the field of mining and economic geology and history of mining with a specialisation in the Kutná Hora ore district. He has cooperated closely with archaeologists who made use of his vast knowledge in the field of medieval mining and metallurgy. The new mineral and its name have been approved by the Commission on New Minerals, Nomenclature and Classification (CNMNC) of the International Mineralogical Association (IMA2022-112; Pažout *et al.* 2023a). Part of the co-type sample has been deposited in the collections of the Department of Mineralogy and Petrology, National Museum, Cirkusová 1740, 193 00 Praha 9, Czech Republic, under the catalogue number P1P 10/2022.

Holubite is a new member of the lillianite group, Strunz class 02.JB.40a, Dana class 3.04.15 and it belongs to the mixed Bi–Sb members of the lillianite homologous series. The structural and chemical features of the lillianite homologues have been described by Makovicky and Karup-Møller (1977). This paper describes the physical and chemical properties of holubite, its crystal structure determined from single-crystal X-ray diffraction data and its relation to other lillianite homologues.

Corresponding author: Richard Pažout; Email: richard.pazout@vscht.cz
Cite this article: Pažout R., Plášil J., Dušek M., Sejkora J. and Dolníček Z. (2023) Holubite, $Ag_3Pb_6(Sb_8Bi_3)_{\Sigma 11}S_{24}$, from Kutná Hora, Czech Republic, a new member of the andorite branch of the lillianite homologous series. *Mineralogical Magazine* **87**, 582–590. https://doi.org/10.1180/mgm.2023.34

Occurrence and sample

Holubite was found in 24 different samples (300 analytical points) from the Staročeské pásmo Lode (Old Bohemian Lode in English)

of the Kutná Hora Ag–Pb–Zn ore district. The ore district (located 60 km east of Prague, Central Bohemia, Czech Republic, 49.9521753N, 15.2634625E) contains a hydrothermal vein type mineralisation of Variscan age (≈ 270 m.y.). The geological situation, mineralogy and geochemistry of the ore district have been detailed by Holub *et al.* (1982) and Malec and Pauliš (1997). It was one of the main European producers of silver in the 14th to 16th Century, with >100 mines on 12 major lodes (Fig. 1). Each lode (ore zone, also called pásmo in Czech or zug in German) represents a hydrothermally altered zone of several hundred metres to ~ 3 km in length and dozens of metres wide, with the depth ranging between several hundred metres to 1 km, each consisting of several, usually parallel veins (Holub *et al.*, 1982). Geologically and mineralogically, two mineral assemblages are present in this ore district, one 'silver-rich' in the southern part of the ore district and one 'pyrite-rich' in the northern part (Malec and Pauliš, 1997). The Staročeské pásmo Lode belongs to the northern pyrite-rich lodes and is the biggest lode of the Kutná Hora ore district. The newly discovered Bi–Ag sulfosalt mineralisation was described in Pažout (2017) and Pažout *et al.* (2017).

All the samples of holubite studied come from the Staročeské pásmo Lode (Old Bohemian Lode) of the Kutná Hora ore district, though Bi was also determined by the first author of this article in sulfosalts from other northern lodes (Hloušecké pásmo Lode and Turkaňské pásmo Lode). The samples were collected in the material from medieval mine dumps, therefore no information is available on their *in situ* position in individual vein structures. Only a small part of the samples studied comes from some recent mining and geological survey activity in the 1960's.

The Staročeské pásmo Lode was mined from the discovery and opening of the ore district in the second half of the 13th Century until the end of large-scale mining at the end of 16th Century. It is estimated that some 350 to 500 t of silver were extracted from this lode, far more than from any other lode of the ore district including the Ag-rich lodes in the South (Malec and Pauliš, 1997). The second peak of mining activity in the Kutná Hora ore district was enabled thanks to the discovery of a new rich deposit, the Benátecká Vein of the Staročeské pásmo Lode, in the second half of the 16th Century. The vein was not discovered by previous miners because it does not crop out. This Ag-rich base-sulfide vein with Fe–Cu–Sn–Zn–As–(Ag–Pb–Bi–Sb) formed mainly of massive pyrite, pyrrhotite, marcasite, chalcopyrite, arsenopyrite, sphalerite and stannite, up to two metres thick, produced an estimated 100 t of silver in <40 years (Holub, 2009). This vein was the

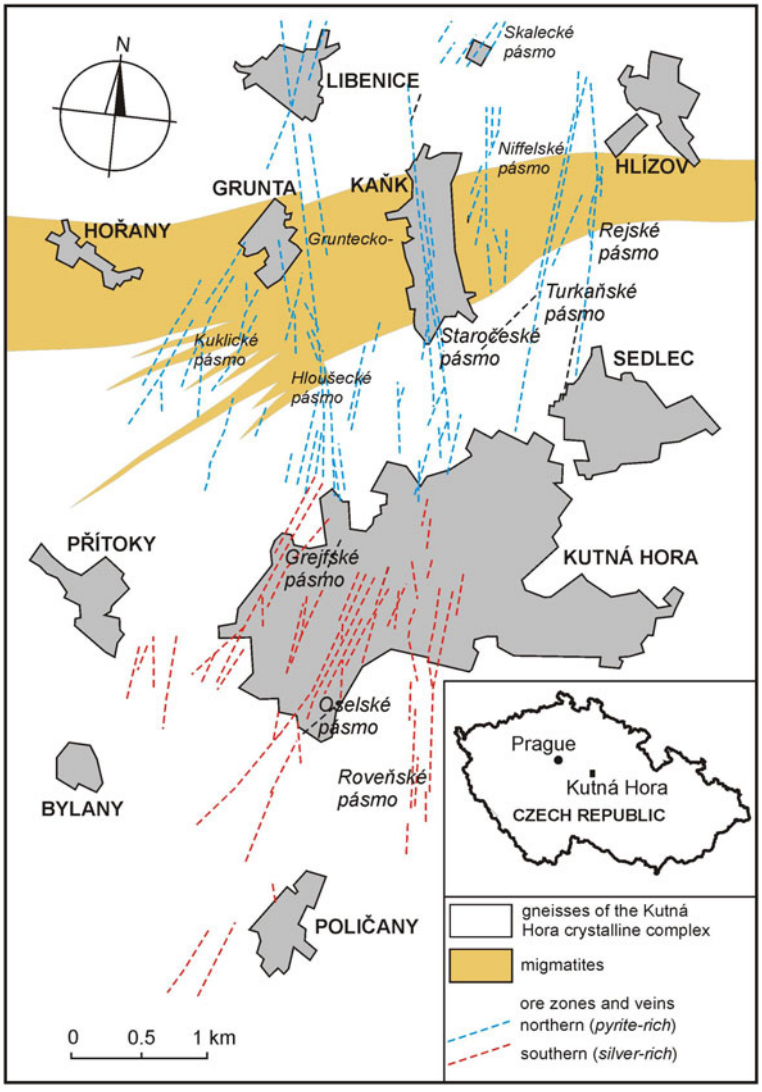

Figure 1. Map of Kutná Hora ore district with major lodes (zones) (Malec and Pauliš, 1997). Each lode (zone) consists of several veins.

https://doi.org/10.1180/mgm.2023.34 Published online by Cambridge University Press

subject of small-scale mining carried out within the Geological Survey in the 1960's and the newly found material from this mining made it possible to study the mineralogical composition of the massive Ag-rich pyrite ores (not present on the medieval dumps), next to Ag–Bi mineralisation in quartz gangue without massive sulfides, which can occasionally be found on mediaeval mine dumps.

The holotype hand sample (ST 61) is formed of white coarse-grained quartz with silvery grey metallic lenses and grains of Ag, Bi-bearing galena and Ag–Bi sulfosalts (including holubite, terrywallaceite, eskimoite and treasurite) up to 3 mm across with no base sulfides. A back-scattered electron (BSE) image of the holotype sample extracted for the structure determination is in Fig. 2. The mineral occurs most frequently as replacement rims and grain aggregates of earlier Ag–Pb–Bi minerals, growing together in aggregates up to 200 × 50 μm. It commonly occurs in a close association with Ag,Bi-bearing galena and terrywallaceite (Fig. 3). We assume the mineral is a replacement product of earlier galena and lillianite homologues, richer in Bi, in line with a general succession trend observed in the Ag–Pb–Bi–Sb mineralisation in the Kutná Hora ore district being from Bi-rich to Sb-rich minerals (Pažout *et. al.*, 2017).

Physical and optical properties

Holubite is opaque, steel-grey in colour and has a metallic lustre and grey streak. The calculated density = 5.899 g.cm^{-3} on the basis of the empirical formula and 5.905 g.cm^{-3} on the basis of the ideal formula, both with single-crystal unit-cell parameters. In reflected light holubite is greyish white and bireflectance and pleochroism are weak with grey tints. Anisotropy is weak to medium, with grey to bluish-grey rotation tints. Fluorescence was not observed, neither were internal reflections. Reflectance values of holubite (WTiC Zeiss 370), measured in air (spectrophotometer MSP400 Tidas at Leica microscope, objective 50×), are in Table 1 (COM standard wavelengths are given in bold) and Fig. 4. A comparison of reflectance curves for holubite, staročeskéite and ramdohrite is in Fig. 5.

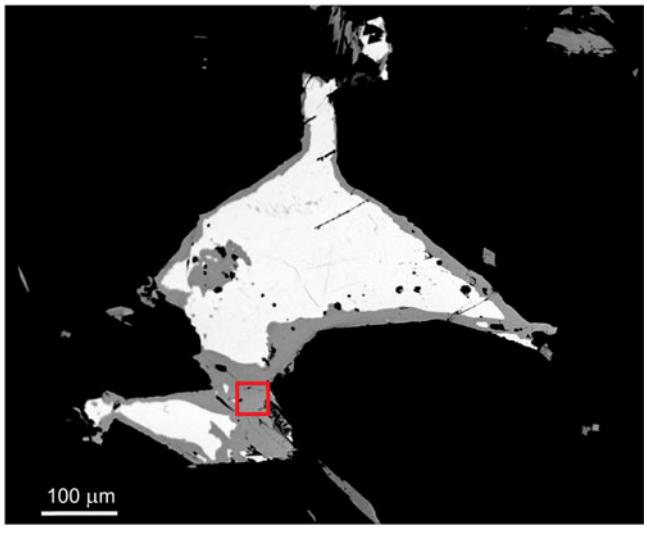

Figure 2. BSE image of holotype sample (ST 61) with Ag,Bi-bearing galena (white) and replacement rims and homogenous grains of holubite (grey). The red box indicates the area sampled for single-crystal X-ray diffraction.

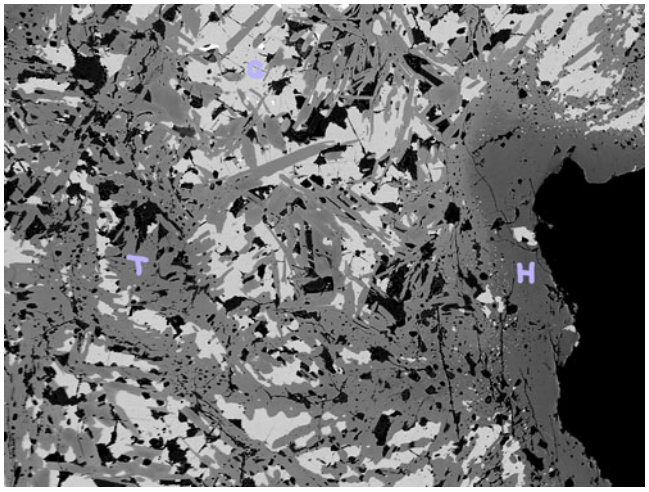

Figure 3. A frequent mode of occurrence of holubite: Ag,Bi-bearing galena (G) replaced by lamellae of terrywallaceite (T, medium grey) and replacement rims of holubite (H, dark grey). The succession is galena – terrywallaceite – holubite. BSE image of sample ST 108; the field of view is 700 μm.

Chemical composition

Chemical analyses of the holotype sample were performed using a JEOL JXA-8600 electron probe microanalyser (EPMA) of University of Salzburg in wavelength dispersive spectroscopy (WDS) mode (25 kV and 35 nA) and beam diameter of 5 μm. The following standards and X-ray lines were used: $CuFeS_2$ (Cu*K*α and Fe*K*α); Ag (Ag*L*α); PbS (Pb*L*α); Bi_2S_3 (Bi*L*α and S*K*α); Sb_2S_3 (Sb*L*α); CdTe (Cd*L*β and Te*L*α); Bi_2Te_2S (Bi*L*α and Te*L*α); and Bi_2Se_3 (Se*K*α). Raw data were corrected with an online ZAF-4 procedure. A second set of polished sections with staročeskéite was measured on a CAMECA SX100 electron probe microanalyser at the National Museum, Prague in 2015. The analytical conditions were as follows: WDS mode, accelerating voltage of 25 kV, beam current of 20 nA, electron-beam diameter of 2 μm and standards: chalcopyrite (S*K*α); Bi_2Se_3 (Bi*M*β); PbS (Pb*M*α); Ag (Ag*L*α); halite (Cl*K*α); Sb_2S_3 (Sb*L*α); CdTe (Cd*L*α); HgTe (Hg*M*α); pyrite (Fe*K*α); Cu (Cu_Kα); ZnS (Zn*K*α); NiAs (As*L*α) and PbSe (Se*L*β). Measured data were corrected using *PAP* software (Pouchou and Pichoir, 1985). Analytical data for the holotype sample are given in Table 2. Its empirical formula (calculated on the basis of 44 atoms per formula unit) is:

$(Ag_{3.03}Cu_{0.03})_{\Sigma 3.06}(Pb_{6.19}Fe_{0.02}Cd_{0.01})_{\Sigma 6.22}(Sb_{7.71}Bi_{2.90})_{\Sigma 10.61}S_{24.12}$, corresponding to $N_{chem} = 4.24$, Bi/(Bi + Sb) = 0.27 and the ($Ag^+ + (Bi^{3+},Sb^{3+}) \leftrightarrow 2\ Pb^{2+}$) substitution percentage $L = 71.6\%$.

Table 1. Reflectance values of holubite (COM standard wavelengths are given in bold).

$R_{min.}$	$R_{max.}$	λ (nm)	$R_{min.}$	$R_{max.}$	λ (nm)
35.9	39.6	400	33.3	36.9	560
36.0	39.8	420	33.0	36.6	580
35.7	39.6	440	**32.7**	**36.4**	**589 (COM)**
35.3	39.1	460	32.6	36.3	600
35.1	**38.9**	**470 (COM)**	32.4	35.9	620
34.8	38.6	480	32.1	35.6	640
34.5	38.3	500	**32.0**	**35.5**	**650 (COM)**
34.0	37.8	520	31.8	35.3	660
33.6	37.3	540	31.5	34.9	680
33.5	**37.2**	**546 (COM)**	31.3	34.6	700

https://doi.org/10.1180/mgm.2023.34 Published online by Cambridge University Press

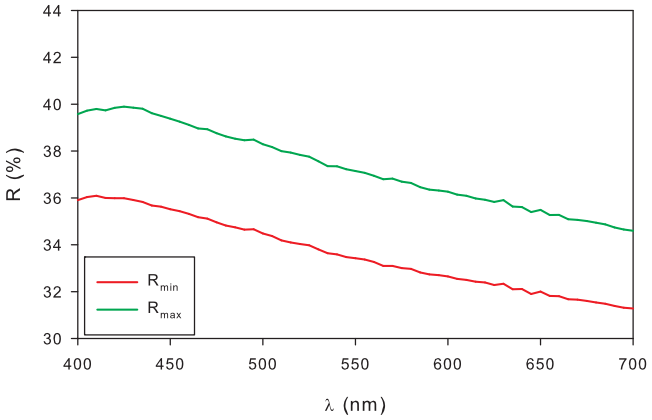

Figure 4. Reflectance curve for holubite from Kutná Hora.

The simplified formula is $(Ag,Cu)_3(Pb,Fe,Cd)_6(Sb_8Bi_3)_{\Sigma 11}S_{24}$ and the ideal formula is $Ag_3Pb_6(Sb_8Bi_3)_{\Sigma 11}S_{24}$, corresponding to (in wt.%) Ag 8.22, Pb 31.58, Sb 24.74, Bi 15.92 and S 19.54, total 100 wt.%. Holubite can be differentiated unequivocally from chemical results from similar members of the lillianite homologous series on the basis of the substitution percentage *L* (calculated from the results of chemical analysis) and the Bi/(Bi+Sb) ratio.

Crystallography and crystal structure

A tiny fragment of holubite with dimensions of 0.035 × 0.030 × 0.030 mm was extracted from a polished section of the holotype sample and separated under the optical stereomicroscope. The intensity data were collected at ambient temperature using an Oxford Diffraction Gemini single-crystal diffractometer equipped with a SuperNova CCD detector and using monochromated Mo*K*α radiation from conventional sealed X-ray tube (55 kV and 30 mA), using a fiberoptics Mo-Enhance collimator. The total of 7038 reflections were measured. After averaging, 4388 reflections were independent and 812 classified as observed [$I_{obs} > 3\sigma(I)$]. Data were corrected for background, Lorentz and polarisation effects, and a multi-scan correction for absorption was applied,

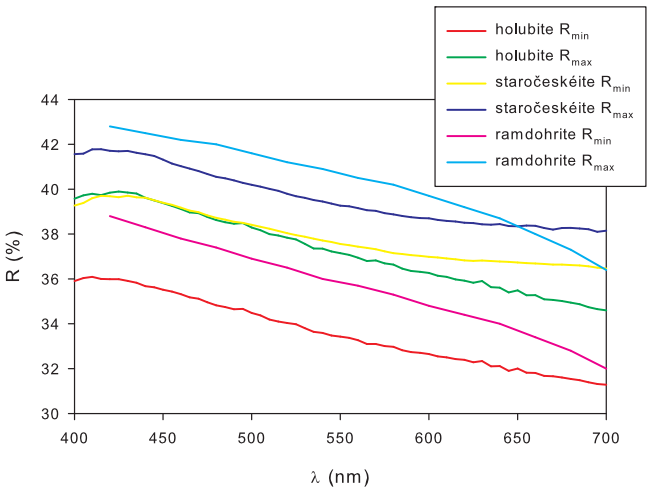

Figure 5. Reflectance curve for holubite from Kutná Hora. For comparison, the curves for staročeskéite from Kutná Hora (Pažout and Sejkora, 2018) and ramdohrite from Chocaya, Bolivia (Picot and Johan, 1982) are shown.

Table 2. Chemical data for holubite (six spot analyses)

Wt.%.	Mean	Range	Standard
Ag	8.34(15)	8.04–8.53	Ag metal
Cu	0.05(3)	0.01–0.10	Cu metal
Fe	0.03(1)	0.02–0.04	FeS_2
Pb	32.76(94)	31.15–33.73	PbS
Cd	0.02(3)	0.00–0.08	CdTe
Sb	23.95(67)	22.71–24.56	Sb_2S_3
Bi	15.47(56)	14.64–16.34	Bi metal
S	19.74(20)	19.42–20.02	$CuFeS_2$
Total	100.36(44)	99.79–101.18	

resulting in R_{int} of the merged data equal to 0.1479. The twinning tool incorporated in *Jana2020* (Petříček *et al.*, 2020) revealed the crystal is twinned on (001) in this unit-cell orientation and the volume fractions of each twin is 0.683(7) and 0.317(7), respectively. The final refinement of occupancies returned values close to those obtained from the microprobe study. The refinement for 122 parameters converged to the final $R = 0.0853$, $wR = 0.1475$ for 812 observed reflections with GOF = 1.31.

In the process of indexing, a monoclinic cell was found; images from data collection showed a primitive unit cell with the presence of reflections doubling the size of the shortest 'sulfosalt' parameter (*c* in this setting), typical of fizélyite, ramdohrite and oscarkempffite. The unit-cell parameters determined from single-crystal data by a least-squares algorithm using the *CrysAlis Pro* package (Rigaku, 2019) are as follows: $a = 19.374(4)$, $b = 13.201(3)$, $c = 8.651(2)$, $\beta = 90.112(18)°$, $V = 2212.5(9)$ Å^3, space group $P2_1/n$ and $Z = 2$. The powder X-ray diffraction data could not be collected due to paucity of material; the calculated powder diffraction data are given in Table 3.

The structure of holubite was solved independently from earlier structure determinations of structurally related compounds by the charge-flipping algorithm (Palatinus and Chapuis, 2007) implemented in *Jana2020* (Petříček *et al.*, 2020). Systematic absences and intensity statistics indicated centrosymmetric space group $P2_1/n$, in line with previous structure determinations of oscarkempffite (Dan Topa, pers. comm.) and ramdohrite (Makovicky *et al.*, 2013). All atomic positions were found, which were subsequently refined by full-matrix least-squares based on F^2 using *Jana2020* (Petříček *et al.*, 2020). The distance and bond-valence calculations indicated that the trigonal prismatic sites Pb2 and Pb3 are occupied solely by Pb, similarly to other known structures of lillianite homologues with $N = 4$ and $L \leq 100\%$. Interatomic distances showed that one of the Sb sites (*M*4) is in a fact a bismuth site which was confirmed by the difference-Fourier and refinement results in *Jana2020* and charge density calculations in the program *ECoN21* (Ilinca, 2022). It also showed that the *M*5 site is a mixed position with ~1:1 ratio of Bi and Ag and that the Sb6 position is a mixed site with 0.86 Sb and 0.14 Pb. Metal atoms were refined with anisotropic atomic displacement parameters (ADPs) with the exception of Sb atoms, which were refined with isotropic ADPs. Due to weak diffraction data (only 812 observed reflections out of the total of 4388 unique reflections), which could not be improved even with an exposition of 400 s per frame and a crystal fragment so small that a shape correction for absorption was not executable, Sb and some S atoms returned negative ADP values at various stages of refinement. However, in the final structural model Sb atoms and all sulfur atoms were successfully refined with individual isotropic ADPs. Details of data collection, crystallographic data and

https://doi.org/10.1180/mgm.2023.34 Published online by Cambridge University Press

Table 3. Calculated powder X-ray diffraction data for holubite. Intensity (I, %) and d_{hkl} (Å) were calculated using the software *Diamond 4* (Putz and Brandenburg, 2017) on the basis of our single-crystal structure refinement. Only reflections with I_{calc} > 3 are listed. The eight strongest reflections are given in bold.

I_{rel} (%)	d (Å)	h	k	l	I_{rel} (%)	d (Å)	h	k	l
3	6.7748	1	$\bar{1}$	1	13	2.0424	4	$\bar{5}$	2
3	6.2479	$\bar{1}$	2	0	13	2.0032	$\bar{4}$	6	0
4	5.8010	$\bar{3}$	1	0	10	1.9374	10	0	0
5	5.4546	$\bar{2}$	2	0	11	1.9133	$\bar{5}$	6	0
4	4.6117	2	$\bar{2}$	1	8	1.9061	$\bar{8}$	3	2
6	4.1105	0	$\bar{1}$	2	9	1.9036	8	$\bar{3}$	2
9	3.9049	$\bar{4}$	2	0	5	1.8489	$\bar{6}$	5	2
21	**3.7864**	**$\bar{2}$**	**$\bar{1}$**	**2**	4	1.8471	6	$\bar{5}$	2
14	3.7814	2	$\bar{1}$	2	18	1.8170	$\bar{5}$	$\bar{2}$	4
27	**3.4706**	**$\bar{3}$**	**$\bar{1}$**	**2**	16	1.8142	5	$\bar{2}$	4
33	**3.4647**	**3**	**$\bar{1}$**	**2**	10	1.8089	0	$\bar{4}$	4
100	**3.3416**	**$\bar{5}$**	**2**	**0**	3	1.8030	$\bar{9}$	4	0
23	**3.3003**	**0**	**4**	**0**	3	1.8014	$\bar{1}$	$\bar{4}$	4
13	3.2534	$\bar{1}$	4	0	3	1.7484	$\bar{7}$	5	2
3	3.2290	6	0	0	3	1.7467	7	$\bar{5}$	2
3	3.0847	0	$\bar{3}$	2	3	1.7220	$\bar{1}$	$\bar{7}$	2
19	3.0470	$\bar{1}$	$\bar{3}$	2	3	1.7217	1	$\bar{7}$	2
15	3.0457	1	$\bar{3}$	2	3	1.7017	$\bar{11}$	2	0
37	**2.9405**	**$\bar{2}$**	**$\bar{3}$**	**2**	10	1.6708	$\bar{10}$	4	0
33	**2.9381**	**2**	**$\bar{3}$**	**2**	5	1.6442	$\bar{1}$	8	0
15	2.9005	$\bar{6}$	2	0	3	1.6267	$\bar{2}$	8	0
17	2.7850	$\bar{3}$	$\bar{3}$	2	4	1.4702	$\bar{4}$	$\bar{6}$	4
22	**2.7820**	**3**	**$\bar{3}$**	**2**	4	1.4690	4	$\bar{6}$	4
10	2.2978	$\bar{7}$	1	2	4	1.4445	$\bar{10}$	0	4
7	2.2938	7	$\bar{1}$	2	3	1.4417	10	0	4
27	2.1627	0	0	4	4	1.4337	$\bar{5}$	$\bar{6}$	4
10	2.1284	$\bar{3}$	$\bar{5}$	2	4	1.4323	5	$\bar{6}$	4
11	2.1271	3	$\bar{5}$	2	3	1.4312	$\bar{12}$	3	2
3	2.1207	$\bar{7}$	4	0	4	1.4019	$\bar{13}$	1	2
14	2.0882	$\bar{8}$	1	2	4	1.4002	13	$\bar{1}$	2
17	2.0848	8	$\bar{1}$	2	3	1.3987	3	$\bar{1}$	6
11	2.0440	$\bar{4}$	$\bar{5}$	2	3	1.3570	$\bar{2}$	$\bar{3}$	6

refinement are given in Table 4. Atom coordinates, occupancies and isotropic displacement parameters are in Table 5, ADPs of metal atoms that were refined anisotropically are in Table 6 and interatomic distances are listed in Table 7. The crystallographic information files have been deposited with the Principal Editor of *Mineralogical Magazine* and are available as Supplementary material (see below). Results of charge-distribution calculations of metal sites in the structure of holubite in the cation-centred description using *ECoN21* (Ilinca, 2022) is in Table 8. The final structural formula is $Ag_{2.98}Pb_{6.28}(Sb_{7.72}Bi_{3.02})_{\Sigma 10.74}S_{24}$, which is in good agreement with microprobe-established composition $(Ag_{3.03}Cu_{0.03})_{\Sigma 3.06}(Pb_{6.19}Fe_{0.02}Cd_{0.01})_{\Sigma 6.22}(Sb_{7.70}Bi_{2.90})_{\Sigma 10.60}S_{24.10}$.

On the basis of the current crystal structure study we conclude that holubite is closely related to ramdohrite, which is a Bi-free lillianite homologue of the andorite branch. Holubite displays two significant differences from ramdohrite, justifying a new mineral species: (1) the marginal octahedral antimony site *Me*6 in ramdohrite (Makovicky *et al.*, 2013) is a bismuth site, Bi4, in holubite; (2) the marginal octahedral *Me*9 site (0.4 Sb + 0.6 Ag) in ramdohrite becomes a Bi–Ag site, *M*5, with 0.51 Bi + 0.49 Ag. In addition, there is one more difference compared to the ramdohrite refinement. The marginal octahedral antimony site *Me*1 in ramdohrite is an Sb–Pb site *M*6 with (0.86 Sb + 0.14 Pb) in holubite, where the excess Pb above 6 apfu is located. Although the issue of excess Pb above 6 apfu (e.g. for And_{70} it is 0.4 Pb) was not addressed in the new refinement of ramdohrite (Makovicky *et al.* 2013), it is likely that either their *Me*1 or *Me*6

Table 4. Summary of data collection conditions and refinement parameters for holubite.

Crystal data	
Structural formula	$Ag_{2.98}Pb_{6.28}Sb_{7.72}Bi_{3.02}S_{24}$
Crystal system	monoclinic
Space group	$P2_1/n$ (Nr.14)
a (Å)	19.374(4)
b (Å)	13.201(3)
c (Å)	8.651(2)
β	90.112(18)
V (Å^3)	2212.5(9)
Z	2
Density (calc.) (g/cm^3)	5.899
F(000)	3365
Crystal size (mm)	0.035 × 0.030 × 0.030
Crystal colour	metallic grey
Data collection	
Temperature (K)	285
Diffractometer	Oxford Diffraction Gemini
Radiation	Mo$K\alpha$, 55kV, 30 mA
Number of frames	120
Measurement time (s/frame)	400
R_{int}	0.1479
Measured reflections	7038
Unique reflections	4388
Observed reflections (I>3 sigma(I))	812
θ_{min} / θ_{max}	2.58/29.42
Range of h, k, l	$-23 \le h \le 26$ $-17 \le k \le 16$ $-9 \le l \le 10$
Refinement	
Refinement on	F^2
R, wR (observed reflections)	0.0853 / 0.1475
R, wR (all reflections)	0.3348 / 0.2855
GoF (observed reflections)	1.3063
GoF (all reflections)	1.0868
No. of least squares parameters	122
No. of constraints	13
Largest difference peak/hole (e^- Å^{-3})	4.68 / −4.68 *

*This value is for sin(th)/lambda limit set to 0.5 (corresponding to d =1 Å).

Table 5. Fractional atomic coordinates, occupancies and equivalent isotropic displacement factors (Å^2).

Atom	x/a	y/b	z/c	$U_{eq/iso}$
Pb1	0.4505(2)	0.6124(3)	0.3704(6)	0.0298(14)
Pb2	0.7512(2)	0.4206(3)	−0.1075(6)	0.0371(16)
Pb3	0.7544(2)	0.4105(4)	0.3908(6)	0.0366(16)
Bi4	0.8526(2)	0.6380(3)	0.6360(6)	0.0329(15)
*M*5*	0.6328(3)	0.6495(4)	0.1131(9)	0.031(2)
*M*6*	0.3759(3)	0.8495(5)	0.6232(9)	0.026(3)
Sb7	0.5572(3)	0.8805(4)	−0.1232(9)	0.0120(15)
Sb8	0.5527(3)	0.8667(5)	0.3651(10)	0.0221(17)
Sb9	0.4482(3)	0.6206(4)	−0.1378(9)	0.0139(15)
Ag10	0.6383(4)	0.6725(7)	0.6216(16)	0.056(4)
S1	0.6677(11)	0.7909(17)	0.354(3)	0.015(5)
S2	0.5179(10)	0.7394(15)	0.569(3)	0.005(5)
S3	0.4109(12)	0.5041(19)	−0.346(4)	0.024(7)
S4	0.7307(11)	0.5475(19)	0.639(3)	0.025(6)
S5	0.3410(11)	0.7274(17)	0.840(3)	0.013(5)
S6	0.5019(12)	0.7634(19)	0.152(3)	0.023(6)
S7	0.7568(12)	0.5630(16)	0.135(3)	0.017(5)
S8	0.6625(16)	0.780(2)	−0.116(4)	0.045(8)
S9	0.3362(12)	0.7318(17)	0.411(3)	0.017(6)
S10	0.9019(13)	0.499(2)	0.421(4)	0.035(8)
S11	0.8965(13)	0.496(2)	0.838(4)	0.027(7)
S12	0.4016(13)	0.522(2)	0.073(4)	0.031(7)

*Site occupation factors: *M*5: $Bi_{0.51(3)}Ag_{0.49(3)}$; *M*6: $Sb_{0.86(4)}Pb_{0.14(4)}$

https://doi.org/10.1180/mgm.2023.34 Published online by Cambridge University Press

Table 6. Anisotropic atomic displacement parameters (in Å^2).

Atom	U^{11}	U^{22}	U^{33}	U^{12}	U^{13}	U^{23}
Pb1	0.0213(19)	0.023(2)	0.045(3)	0.0006(19)	0.001(2)	−0.002(3)
Pb2	0.034(2)	0.031(3)	0.046(3)	−0.005(2)	−0.004(3)	0.011(3)
Pb3	0.033(2)	0.043(3)	0.034(3)	−0.009(2)	0.006(3)	−0.005(3)
Bi4	0.032(2)	0.033(2)	0.034(3)	0.001(2)	0.000(2)	0.003(3)
*M*5	0.022(3)	0.019(3)	0.053(5)	0.003(2)	0.011(3)	−0.003(3)
Ag10	0.035(5)	0.054(6)	0.080(9)	0.024(5)	−0.016(6)	−0.004(7)

Table 7. Selected interatomic distances (Å).

Pb1–S2	2.73(2)	Bi4–S4	2.65(2)
Pb1–S3	2.94(3)	Bi4–S5	3.13(3)
Pb1–S3	3.10(2)	Bi4–S6	3.18(2)
Pb1–S6	2.92(3)	Bi4–S9	2.95(3)
Pb1–S9	2.74(2)	Bi4–S10	2.79(3)
Pb1–S12	2.99(3)	Bi4–S11	2.70(3)
Pb2–S1	3.19(3)	Bi5,Ag5–S1	2.88(3)
Pb2–S4	2.79(3)	Bi5,Ag5–S3	2.98(3)
Pb2–S5	3.52(2)	Bi5,Ag5–S6	2.97(2)
Pb2–S7	2.82(2)	Bi5,Ag5–S7	2.67(2)
Pb2–S8	3.46(3)	Bi5,Ag5–S8	2.69(3)
Pb2–S9	3.71(3)	Bi5,Ag5–S12	2.86(3)
Pb2–S11	3.02(3)		
Pb2–S12	3.07(3)		
Pb3–S1	3.04(3)	Sb6,Pb6–S2	3.15(2)
Pb3–S3	3.42(2)	Sb6,Pb6–S5	2.56(3)
Pb3–S4	2.85(3)	Sb6,Pb6–S7	2.58(2)
Pb3–S5	3.27(2)	Sb6,Pb6–S9	2.53(3)
Pb3–S7	2.99(2)	Sb6,Pb6–S10	3.30(3)
Pb3–S8	3.06(3)	Sb6,Pb6–S11	3.23(3)
Pb3–S9	3.09(2)		
Pb3–S10	3.10(3)		
Sb8–S1	2.44(2)	Sb7–S2	3.34(2)
Sb8–S2	2.53(2)	Sb7–S6	3.04(3)
Sb8–S6	2.49(3)	Sb7–S8	2.44(3)
Sb8–S10	3.15(3)	Sb7–S10	2.47(3)
Sb8–S11	3.23(3)	Sb7–S10	3.43(3)
Sb8–S11	3.54(3)	Sb7–S11	2.57(3)
Sb9–S2	3.28(2)	Ag10–S1	2.85(3)
Sb9–S3	2.48(3)	Ag10–S2	2.53(2)
Sb9–S5	2.52(2)	Ag10–S3	3.47(3)
Sb9–S6	3.30(3)	Ag10–S4	2.44(3)
Sb9–S12	2.42(3)	Ag10–S8	2.72(4)
Sb9–S12	3.51(3)	Ag10–S12	3.77(3)

site (or both) contain some Pb. A similar situation is in the structure of andorite IV (Nespolo *at al.*, 2012), where authors did not address the issue of excess Pb above 4 apfu (e.g. for $And_{92.5}$ it is 0.6 Pb).

The structure of holubite, a natural Sb–Bi monoclinic ^{4,4}L homologue of the lillianite homologous series, contains 10 cation (metal) sites and 12 anion (sulfur) sites. The metal sites consist of two Pb sites (Pb2 and Pb3) in trigonal prismatic coordination and eight independent octahedral sites. Four of the octahedral sites are marginal octahedra flanking the bicapped trigonal prisms of Pb2 and Pb3 from each side along *a* and four are central octahedra inside the ^{4}L slabs. Both types of octahedra (marginal and central) can be viewed as formed by two rows along *c*, each row consisting of two alternating metal sites. The structure of holubite projected down [001] is shown in Fig. 6.

Regarding the marginal octahedra, in one row the Ag site Ag10 alternates with the Ag–Bi mixed site *M*5 (0.51Bi + 0.49Ag), in the other row one Pb–Sb mixed site *M*6 (0.86 Sb – 0.14 Pb) alternates with the pure Bi site Bi4. This is a significant difference compared to ramdohrite (Makovicky *et al.*, 2013). In ramdohrite along *a* (in their setting), in one row the Ag site *Me*4 alternates with the Ag–Sb mixed site *Me*9 (0.4 Sb + 0.6 Ag), while in the other pure Sb site *Me*1 alternates with the Sb site *Me*6. On the other hand, this situation in holubite is somewhat similar (owing to the presence of the Sb–Pb site) to the one in the structure of Ag-excess fizélyite (Yang *et al.*, 2009), where one row of octahedra is formed by two alternating Sb positions Sb1 and Sb3. The situation in the second row is more complex here as there is alternation between a partially occupied pair Ag1 (0.75Ag) and Ag1' (0.19Ag) with a *M*2 and *M*2' mixed pair. *M*2' is formed by partially occupied Ag (0.33Ag), whereas *M*2 contains (0.556Pb + 0.095Sb). Furthermore, there is another partially occupied position Ag2 (0.21Ag) sandwiched between the two pairs, not detected in structures of other andorite-branch minerals. As to the central octahedra, the situation in holubite and ramdohrite is similar. In holubite, one row is formed by alternating Sb positions Sb7 and Sb8 (pure Sb sites *Me*2 and *Me*7 in ramdohrite), while in the other the Pb site Pb1 alternates with the pure Sb site Sb9 (the Pb site *Me*5 alternates with the Sb site *Me*10 in ramdohrite). All four Sb sites in holubite are typical pure Sb sites with three short and three long opposing distances. The coordination of Bi4 does not deviate from a pure Bi site in other sulfosalts and the same applies to the octahedral Pb site Pb1.

Table 8. Detailed results of charge-distribution calculations of metal sites in the structure of holubite in the cation-centred description using the program *ECoN21* (Ilinca, 2022).

Cation	Site population	CN	ECoN	EDEV	AV	PVol	qX	QX	qX/QX	MAPDL	BVS
Pb1	1.00.Pb	6	5.581	0.070	2.905	31.426	2.000	2.116	0.945	6.842	2.392
Pb2	1.00.Pb	8	5.581	0.302	3.198	55.990	2.000	1.962	1.019	3.971	1.864
Pb3	1.00.Pb	8	7.313	0.086	3.102	52.178	2.000	1.953	1.024	5.011	1.920
Bi4	1.00.Bi	6	5.021	0.163	2.897	31.155	3.000	2.992	1.003	5.472	2.854
*M*5	0.51.Bi/0.49.Ag	6	5.610	0.065	2.840	29.652	2.020	2.024	0.998	4.524	2.005
*M*6	0.86.Sb/0.14.Pb	6	3.501	0.416	2.891	31.138	2.860	2.703	1.058	6.328	2.880
Sb7	1.00.Sb	6	3.259	0.457	2.879	30.944	3.000	3.018	0.994	5.917	3.279
Sb8	1.00.Sb	6	3.177	0.365	2.899	31.719	3.000	3.202	0.937	5.059	3.236
Sb9	1.00.Sb	6	3.038	0.392	2.916	32.558	3.000	3.009	0.997	8.100	3.335
Ag10	1.00.Ag	6	3.532	0.294	2.962	31.514	1.000	1.021	0.979	4.745	1.121

Key: MAPD: 2.58%; CN – coordination number; ECoN – effective coordination number; EDEV – deviation of ECoN from CNR (number of ligands with bond weights exceeding 0.001); AV– average bond length; PVol – volume of coordination polyhedron; qX – oxidation number of cations; QX – charge received by cations; MAPDL – mean absolute percentage deviation of ligands QA (anion charge); MAPD – mean absolute percentage deviation of QX; BVS – bond valence sum.

https://doi.org/10.1180/mgm.2023.34 Published online by Cambridge University Press

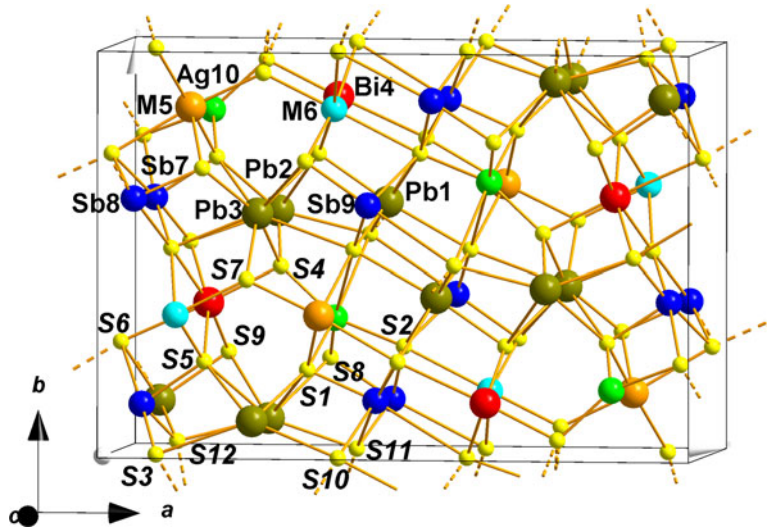

Figure 6. The crystal structure of holubite, a natural Bi–Sb ^{4,4}L homologue of the lillianite homologous series: Pb2 and Pb3 – lead atoms in bicapped trigonal prismatic coordination (CN 8), all other metal atoms are in octahedral coordination (CN 6). Marginal octahedra are: Ag10, *M*5 (Bi–Ag mixed site), Bi4 and *M*6 (Sb6–Pb6 mixed site). Central octahedral are: Pb1, Sb9, Sb8 and Sb7, S – sulfur atoms. View down *c* axis. Holubite is closely related to ramdohrite (Makovicky *et al*., 2013) and oscarkempffite (Topa, personal communication). Drawn using *Diamond 4* (Putz and Brandenburg, 2017).

Relation to other species

Holubite is a new member of the lillianite homologous series, class 3.1.1. of the Sulfosalt systematics (Moëlo *et al.*, 2008), Strunz class 02.JB.40a, Dana class 3.04.15. A comparison of selected data for holubite $Ag_3Pb_6(Sb_8Bi_3)_{\Sigma 11}S_{24}$, ramdohrite $Ag_3Pb_6Sb_{11}S_{24}$ and staročeskéite $Ag_{0.70}Pb_{1.60}(Bi_{1.35}Sb_{1.35})_{\Sigma 2.70}S_6$ is given in Table 9. All three minerals display the same (or very similar) percentage of the lillianite substitution [$Ag^+ + (Bi^{3+},Sb^{3+}) \leftrightarrow 2\ Pb^{2+}$], $L\% \approx 70$ and only differ by Bi content substituting for Sb. Whereas ramdohrite is a pure Sb member with no bismuth, holubite has one quarter to one third of Sb replaced by Bi (Bi/(Bi+Sb) = 0.26–0.34) and staročeskéite has a half of the Sb content replaced by Bi (Bi/(Bi+Sb) ≈ 0.5).

Structurally, holubite has a unit cell and symmetry similar to those of ramdohrite, fizélyite, Ag-rich fizélyite, uchucchacuaite, menchettiite, oscarkempffite (Makovicky and Topa, 2014) and lazerckerite, with $a \approx 19$, $b \approx 13$, $c \approx 8.5$, $\beta \approx 90°$, $V \approx 2200$, (regardless of axial setting) and space group $P2_1/n$ or $P2_1/c$. Lazerckerite, $Ag_{3.75}Pb_{4.50}(Sb_{7.75}Bi_4)S_{24}$, is a new mineral of the andorite branch, of the lillianite homologous series with $L\% \approx$ 90–95 and a Bi/(Bi+Sb) ratio of ~0.30 (IMA2022-113; Pažout *et al.* 2023b). Chemically, holubite can be compared with other related lillianite homologues on the basis of two parameters: (1) lillianite substitution percentage *L*%; and (2) bismuth (vs. antimony) content expressed as the Bi/(Bi+Sb) ratio. Regarding the *L*% – holubite has the same *L*% as ramdohrite and staročeskéite (all three have $L\% \approx 70$). However, ramdohrite has no bismuth, whereas holubite has Bi/(Bi+Sb) = 0.26–0.34 and staročeskéite has Bi/(Bi+Sb) = 0.45–0.55. Regarding the Bi/(Bi+Sb) ratio – three minerals display Bi/(Bi+Sb) of ~0.30: holubite, lazerckerite and oscarkempffite. However, holubite has $L\% \approx 70$, lazerckerite has $L\% \approx$ 90–95 and oscarkempffite is even an over-substituted member with $L\% \approx$ 120–125. All these minerals possess the above monoclinic unit cell with the exception of staročeskéite, which has an orthorhombic unit cell with $a \approx 19$, $b \approx 13$, $c \approx 4.25$ and $V \approx 1100$ (regardless of axial setting). Thus holubite stands as a unique mineral both structurally and chemically, differing distinctly from ramdohrite, staročeskéite, lazerckerite and oscarkempffite and other known members of the lillianite homologous series. It is defined as a lillianite homologue with the following requirements: $N = 4$, L ($Ag^+ + Bi^{3+},Sb^{3+} \leftrightarrow 2Pb^{2+}$

Table 9. Comparative data for the relevant minerals.

	Holubite	Ramdohrite	Staročeskéite
Locality	Kutná Hora, Czech Republic	Potosí, Bolivia	Kutná Hora, Czech Republic
Reference	this paper	Makovicky *et al.* (2013)	Pažout and Sejkora (2018)
Ideal composition	$Ag_3Pb_6(Sb_8Bi_3)_{\Sigma 11}S_{24}$	$Ag_3Pb_6Sb_{11}S_{24}$	$Ag_{0.70}Pb_{1.60}(Bi_{1.35}Sb_{1.35})_{\Sigma 2.70}S_6$
Empirical composition	$(Ag_{3.03}Cu_{0.03})_{\Sigma 3.06}(Pb_{6.19}Fe_{0.02}Cd_{0.01})_{\Sigma 6.22}$ $Sb_{7.71}Bi_{2.90})_{\Sigma 10.61}S_{24.12}$	$Pb_{5.9}Fe_{0.1}Mn_{0.1}In_{0.1}Cd_{0.2}Ag_{2.8}Sb_{10.8}S_{24}$	$Ag_{0.69}Pb_{1.56}(Bi_{1.32}Sb_{1.37})_{\Sigma 2.69}$ $(S_{6.04}Se_{0.01})_{\Sigma 6.05}$
Space group	$P2_1/n$	$P2_1/n$	*Cmcm*
a (Å)	19.374(4)	8.7348(3)	4.2539(8)
b (Å)	13.201(3)	13.0543(4)	13.3094(8)
c (Å)	8.651(2)	19.3117(6)	19.625(1)
β (°)	90.112(18)	90.179(2)	
V (Å^3)	2212.5(9)	2202.04	1111.1(2)
Z	2	2	4
Strongest lines in the XRD powder pattern *d* (Å) / *I* (%)	3.786/21*	3.802/30*	3.746/33*
	3.471/27	3.488/37	3.446/62
	3.342/100	3.478/32	3.382/100
	3.035/45	3.324/100	3.035/45
	2.941/37	2.935/58	2.932/81

*– calculated from the structure data

https://doi.org/10.1180/mgm.2023.34 Published online by Cambridge University Press

substitution) ≈ 70% and about one quarter to one third at.% of antimony is replaced by bismuth (Bi/(Bi+Sb) ≈ 0.26–0.34).

Mixed members of the lillianite homologous series are either Bi–Sb members or Sb–As members (arsenquatrandorite and jasrouxite). Here we will deal with the former. The mixed Bi–Sb members of the lillianite homologous series is a fairly new and not so frequent group among either Bi-dominant (lillianite branch) or Sb-dominant (andorite branch) members of the series. To this date, it comprises four minerals: terrywallaceite, oscarkempffite, clino-oscarkempffite and staročeskéite, which is now being widened by the addition of holubite and lazerckerite (IMA2022-113). Oscarkempffite $Pb_4Ag_{10}Sb_{17}Bi_9S_{48}$ is characterised by $L = 120–125\%$ and a Bi/(Bi+Sb) range between 0.29 and 0.37 (Topa *et al.*, 2016), clino-oscarkempffite $Pb_6Ag_{15}Sb_{21}Bi_{18}S_{72}$ has $L = 122–123\%$ and Bi/(Bi+Sb) = 0.46–0.48 (Makovicky *et al.*, 2017). Terrywallaceite has $L = 80–110\%$ and Bi/(Bi+Sb) = 0.45–0.75 (values obtained by EPMA, Pažout, 2017).

Notable occurrences of mixed Bi–Sb members with $N = 4$ (both Sb-rich members of the lillianite branch and Bi-rich members of the andorite branch) were previously described on the basis of the EPMA data from Alyaskitovoye deposit, Yakutia, Russia (Mozgova *et al.*, 1987, 1988), from Julcani, Peru (Moëlo *et al.*, 1989) and Oruro, Bolivia (Keutsch and Brodtkorb, 2008). Recently, an extraordinary extent of the Bi–Sb substitution in minerals of the lillianite homologous series was described from the Kutná Hora ore district, Czech Republic (Pažout, 2017). Due to a lack of single-crystal data (resulting from the difficulty to find suitable homogenous grains) these Bi–Sb members were then characterised in Pažout (2017) as Bi-rich fizélyite or Bi-rich ramdohrite (= holubite, IMA2022-112) and Bi-rich andorite IV (= lazerckerite, IMA2022-113).

Comparing the data from Kutná Hora with published data from elsewhere in the past, it is apparent that a mineral phase corresponding to holubite has not been described before. Mineral phases from Alyaskitovoye deposit (Mozgova *et al.*, 1987, 1988) show L% between 94 and 114 and Bi/(Bi+Sb) = 0.41–0.70, and thus correspond mainly to terrywallaceite, which is also supported by their diffraction data. Samples from Julcani (Moëlo *et al.*, 1989) with L% = 101–118 and Bi/(Bi+Sb) = 0.31–0.40 correspond to a phase that can be chemically characterised as Bi-rich andorite VI (analyses with L% ≈ 101 and Bi/(Bi+Sb) around 0.30), terrywallaceite (analyses with L% ≈ 100–115 and Bi/(Bi+Sb) > 0.40) or oscarkempffite (analyses with L% ≈ 118). The majority of analyses show L% between 105 and 115; precise identification of these minerals would be possible on the basis of structural characterisation by single-crystal diffraction. Samples from Oruro (Keutsch and Brodtkorb, 2008) with L% = 94.4 and Bi/(Bi+Sb) = 0.23 correspond to lazerckerite (IMA2022-113).

The question arises how to evaluate samples from Kutná Hora with border values of Bi/(Bi+Sb), which for holubite with L% ≈ 70 is 0.19 and 0.45 (values encountered by EPMA by the first author of this article). The value of 0.19 still corresponds in all cases to holubite, whether the depletion of Bi occurs in $M5$ site (Ag increases, Bi decreases) or in the Bi4 site (which would become a Bi–Sb site with Bi ≥ Sb). Analytical points with the value of 0.45 are difficult to classify, because these fall in the substitution field of staročeskéite. Hypothetically, if all Ag in $M5$ is replaced by bismuth, Bi/(Bi+Sb) is equal to 0.36 then we may still deal with holubite. A further increase in Bi content would result most probably in one (or more) Sb sites to become an Sb–Bi mixed site with Sb ≥ Bi and the question arises whether such a phase would keep the a ≈ 19, b ≈ 13, c ≈ 8.5, β ≈ 90° and V ≈ 2200 cell of holubite or acquire the a ≈ 19, b ≈ 13, c ≈ 4.25 and V ≈ 1100 cell of staročeskéite (Pažout and Dušek, 2010). This question can be answered only by single-crystal X-ray diffraction which could show unequivocally whether the halving of the 4.25 Å periodicity occurs or not.

Acknowledgements. The authors thank Dan Topa for the WDS measurements. This work was financed by the Czech Science Foundation (GAČR project 15-18917S) to RP and by the Ministry of Culture of the Czech Republic (long-term project DKRVO 2019-2023/1.II.e; National Museum, 00023272) for JS and ZD. The helpful comments of an anonymous reviewer, Peter Leverett, Panagiotis Voudouris, Associate Editor Oleg I Siidra and Principal Editor Stuart Mills are greatly appreciated.

Supplementary material. The supplementary material for this article can be found at https://doi.org/10.1180/mgm.2023.34.

Competing interests. The authors declare none.

References

Holub M. (2009) Estimate of the amount of silver in ores mined from Staročeské pásmo Lode – Contributions to the history of silver mining. *Kutnohorsko - vlastivědny sborník*, **11**, 30–56 [in Czech].

Holub M., Hoffman V., Mikuš V. and Trdlička Z. (1982) Polymetallic mineralization of the Kutná Hora ore district. *Sborník geologických věd, ložisková geologie, mineralogie*, **23**, 69–123 [in Czech].

Ilinca G. (2022) Charge distribution and bond valence sum analysis of sulfosalts – The ECoN21 computer program. *Minerals*, **12**, 924.

Keutsch F. and Brodtkorb M.K. (2008) Metalliferous paragenesis of the San José mine, Oruro, Bolivia. *Journal of South American Earth Sciences*, **25**, 485–491.

Makovicky E. and Karup-Møller S. (1977) Chemistry and crystallography of the lillianite homologous series, part I. General properties and definitions. *Neues Jahrbuch für Mineralogie, Abhandlungen*, **130**, 265–287.

Makovicky E. and Topa D. (2014) Lillianites and andorites: new life for the oldest homologous series of sulfosalts. *Mineralogical Magazine*, **78**, 387–414.

Makovicky E., Mumme W.G. and Gable R.W. (2013) The crystal structure of ramdohrite, $Pb_{5.9}Fe_{0.1}Mn_{0.1}In_{0.1}Cd_{0.2}Ag_{2.8}Sb_{10.8}S_{24}$: A new refinement. *American Mineralogist*, **98**, 773–779.

Makovicky E., Topa D. and Paar W.H. (2017) The definition and crystal structure of clino-oscarkempffite, $Ag_{15}Pb_6Sb_{21}Bi_{18}S_{72}$. *European Journal of Mineralogy*, **29**, 1–11.

Malec J. and Pauliš P. (1997) Kutná Hora ore mining district and appearances of past mining and metallurgic activities on its territory. *Bulletin Mineralogicko-petrologického oddělení Národního muzea v Praze*, **4–5**, 86–105 [in Czech with English abstract].

Moëlo Y., Makovicky E. and Karup-Møller S. (1989) Sulfures complexes plombo argentiféres : minéralogie et cristallochimie de la série andorite–fizélyite, $(Pb,Mn,Fe,Cd,Sn)_{3-2x}(Ag,Cu)_x(Sb,Bi,As)_{2+x}(S,Se)_6$. *Documents du BRGM*, **167**, 1–107.

Moëlo Y., Makovicky E., Mozgova N., Jambor J., Cook N., Pring A., Paar W., Nickel E., Graeser S., Karup-Møller S., Balić-Žunić T., Mumme W., Vurro F., Topa D., Bindi L., Bente K., Shimizu M. (2008). Sulfosalt systematics: A review. Report of the sulfosalt sub-committee of the IMA Commission on Ore Mineralogy. *European Journal of Mineralogy*. **20**. 7–46.

Mozgova N.N., Nenasheva S.N., Borodaev J.S., Sivcov A.V., Ryabeva E.G. and Gamayanin G.N. (1987) New mineral varieties in sulfosalts group. *Zapiski Vsesoyuznogo Mineralogicheskogo Obshchestva*, **116**, 614–28 [in Russian].

Mozgova N.N., Nenasheva S.N., Jefimov A.V., Borodaev S., Cepin A.I. and Sivcov A.V., (1988): New data about antimony-bismuth lillianite homologues. *Mineralogicheskij Zurnal*, **10**, 35–45 [in Russian].

Nespolo M., Ozawa T., Kawasaki Y. and Sugiyama K. (2012) Structural relations and pseudosymmetries in the andorite homologous series. *Journal of Mineralogical and Petrological Sciences*, **107**, 226–243.

Palatinus L. and Chapuis G. (2007) Superflip – a computer program for the solution of crystal structures by charge flipping in arbitrary dimensions. *Journal of Applied Crystallography*, **40**, 786–790.

Pažout R. (2017) Lillianite homologues from Kutná Hora ore district, Czech Republic: a case of large-scale Sb for Bi substitution. *Journal of Geosciences*, **62**, 37–57.

Pažout R. and Dušek. M. (2010) Crystal structure of natural orthorhombic $Ag_{0.71}Pb_{1.52}Bi_{1.32}Sb_{1.45}S_6$, a lillianite homologue with N = 4; comparison with gustavite. *European Journal of Mineralogy*, **22**, 741–750.

Pažout R. and Sejkora J. (2018) Staročeskéite, $Ag_{0.70}Pb_{1.60}(Bi_{1.35}Sb_{1.35})_{\Sigma 2.70}S_6$, from Kutná Hora, Czech Republic, a new member of lillianite homologous series. *Mineralogical Magazine*, **82**, 993–1005.

Pažout R., Sejkora J. and Šrein V. (2017) Bismuth and bismuth–antimony sulfosalts from Kutná Hora vein Ag–Pb–Zn ore district, Republic. *Journal of Geosciences*, **62**, 59–76.

Pažout R., Plášil J., Dušek M., Sejkora J. and Dolníček Z. (2023a) Holubite, IMA 2022-112. CNMNC Newsletter 72. *Mineralogical Magazine*, **87**, 512–518, https://doi.org/10.1180/mgm.2023.21.

Pažout R., Plášil J., Dušek M., Sejkora J. and Ilinca G. (2023b) Lazerckerite, IMA 2022-113. CNMNC Newsletter 72. *Mineralogical Magazine*, **87**, 512–518, https://doi.org/10.1180/mgm.2023.21.

Petříček V., Dušek M. and Palatinus L. (2020) *Crystallographic computing system Jana2020*. Institute of Physics, CAS, Prague, Czech Republic.

Picot P. and Johan Z. (1982) *Atlas of Ore Minerals*. B.R.G.M. Orléans, 458 pp.

Pouchou J.L. and Pichoir F. (1985) "PAP" (φρZ) procedure for improved quantitative microanalysis. Pp. 104–106 in: *Microbeam Analysis* (J.T. Armstrong, editor). San Francisco Press, San Francisco.

Putz H. and Brandenburg K. (2017) *Diamond – crystal and molecular structure visualization*. Crystal Impact-GbR, Bonn, Germany.

Rigaku (2019) *CrysAlis CCD and CrysAlis RED*. Rigaku–Oxford Diffraction Ltd, Yarnton, Oxfordshire, UK.

Topa D., Makovicky E., Stanley C.J. and Robetzs A.C. (2016) Oscarkempffite, $Ag10Pb4(Sb_{17}Bi_9)_{\Sigma 26}S_{48}$, a new Sb–Bi member of the lillianite homologous series. *Mineralogical Magazine*, **80**, 809–817.

Yang H., Downs R.T., Burt J.B. and Costin G. (2009) Structure refinement of an untwinned single crystal of Ag-excess fizelyite, $Ag_{5.94}Pb_{13.74}Sb_{20.84}S_{48}$. *The Canadian Mineralogist*, **47**, 1257–1264.

https://doi.org/10.1180/mgm.2023.34 Published online by Cambridge University Press